

Ultraluminous and Hyperluminous Infrared Galaxies in the SDSS, 2dFGRS and 6dFGS

Ho Seong Hwang,^{1,2*} Stephen Serjeant,^{3,4} Myung Gyoon Lee¹,
Kang Hwan Lee,^{3,5} and Glenn White^{4,6}

¹*Astronomy Program, Department of Physics and Astronomy, FPRD, Seoul National University, Seoul 151-742, Korea*

²*Visiting Research Associate, Centre for Astrophysics & Planetary Science, School of Physical Sciences, University of Kent, Canterbury, Kent CT2 7NR*

³*Centre for Astrophysics & Planetary Science, School of Physical Sciences, University of Kent, Canterbury, Kent CT2 7NR*

⁴*Astrophysics Group, Department of Physics and Astronomy, The Open University, Milton Keynes MK7 6AA*

⁵*National Science Museum Planning Office, Ministry of Science & Technology, Gwacheon Kyungi, 427-715, Korea*

⁶*CCLRC Rutherford Appleton Laboratory, Chilton, Didcot, Oxfordshire OX11 0QX*

12 October 2018

ABSTRACT

We present a result of cross-correlating the *Infrared Astronomical Satellite* Faint Source Catalogue (*IRAS* FSC) with the spectroscopic catalogues of galaxies in the Fourth Data Release of Sloan Digital Sky Survey (SDSS), the Final Data Release of 2dF Galaxy Redshift Survey (2dFGRS) and the Second Data Release of 6dF Galaxy Survey (6dFGS). We have identified 324 ultraluminous infrared galaxies (ULIRGs) including 190 newly discovered ULIRGs, and 2 hyperluminous infrared galaxies (HLIRGs). Adding these new ULIRGs, we increase the number of known ULIRGs by about 30 per cent. The reliability of the cross-correlation is estimated using the likelihood ratio method. The incompleteness of our sample introduced by the identification procedure in this study is estimated to be about 5 per cent. Our sample covers the redshift range of $z=0.037-0.517$ with a median redshift of $\bar{z}=0.223$, which is larger than that ($\bar{z}=0.184$) of the sample of previously known ULIRGs.

Key words: galaxies: active – galaxies: general – infrared: galaxies

1 INTRODUCTION

The interest in luminous infrared galaxies, in particular ultraluminous infrared galaxies¹ (ULIRGs) and the hyperluminous infrared galaxies² (HLIRGs), has been growing since the launch of *Infrared Astronomical Satellite* (*IRAS*; Neugebauer et al. 1984) in 1983. A great deal of effort has been made to understand the origin of the enormous infrared luminosities of these populations and the time evolution of individual ULIRGs, which are summarised in Sanders & Mirabel (1996) and Lonsdale, Farrah, & Smith (2006). It is generally accepted that dust heated by some combination of starburst and active galactic nuclei (AGN) activity is responsible for the IR luminosity (e.g. Farrah et al. 2003). However, it is not yet clear which is

the dominant power source. There are several suggestions for the time evolution of individual ULIRGs. Sanders et al. (1988a) suggested that ULIRGs may be an initial, dust-shrouded stage of optical QSOs, while Farrah et al. (2001) proposed that ULIRGs are not a simple transition stage from galaxy mergers to QSOs but evolve through diverse paths. On the other hand, several authors suggested that ULIRGs might evolve into moderately massive (L^*) field ellipticals (Kormendy & Sanders 1992; Genzel et al. 2001; Tacconi et al. 2002).

Infrared space telescopes have driven much recent progress (see Genzel & Cesarsky 2000 and Verma et al. 2005 for a review). Genzel et al. (1998) showed that several diagnostic lines in mid-infrared spectra using *Infrared Space Observatory* (*ISO*; Kessler et al. 1996) are very powerful in characterizing the power source of ULIRGs. They concluded that most ULIRGs (80%) are powered by starbursts, but at least half of their sample require both a starburst and an AGN. Similar results are found in Lutz et al. (1998) and Rigopoulou et al. (1999). Moreover, Tran et al. (2001) showed that ULIRGs with $L_{ir} < 10^{12.4} L_{\odot}$ are mostly

* E-mail: hshwang@astro.snu.ac.kr

¹ We define ULIRGs as the galaxies whose infrared (1–1000 μm) luminosities are greater than $10^{12} L_{\odot}$.

² We define HLIRGs as the galaxies whose infrared luminosities are greater than $10^{13} L_{\odot}$.

starburst dominated, while ULIRGs with $L_{ir} > 10^{12.4} L_{\odot}$ more likely to contain AGN. The *Spitzer Space Telescope* (Werner et al. 2004) and submillimetre/millimetre-wave cameras such as *SCUBA* are now extending samples of ULIRGs to higher redshifts ($z > 1$). Several authors (Houck et al. 2005; Lutz et al. 2005; Yan et al. 2005) took spectra of optically faint and infrared luminous population using *Spitzer*, detecting broad spectral features such as PAH (Polycyclic Aromatic Hydrocarbon) emission and silicate absorption. They showed that the majority of these population are at high redshift ($z \sim 2$) and have mid-infrared spectral shapes similar to local AGN-dominated ULIRGs.

Since the publication of the *IRAS* Point Source Catalogue (1988; hereafter PSC) and the *IRAS* Faint Sources Catalogue – Version 2 (Moshir et al. 1992, hereafter FSC92), many wide-area redshift survey follow-up campaigns have been conducted. In total, these have led to a heterogeneous compilation of a few hundred ULIRGs from sources such as the IRAS 1.2 Jy Redshift Survey (Strauss et al. 1990, 1992; Fisher et al. 1995), the IRAS 1 Jy Survey of ULIRGs (Kim & Sanders 1998), the QDOT all-sky IRAS galaxy redshift survey (Lawrence et al. 1999), the Point Source Catalogue redshift survey (Saunders et al. 2000), the FIRST/FSC sample (Stanford et al. 2000), and the Revised Bright Galaxy Sample³ (Sanders et al. 2003). The small area surveys are summarised in Sanders & Mirabel (1996) and Lonsdale, Farrah, & Smith (2006). The majority of ULIRGs found in all sky redshift surveys are from the nearby universe ($z < 0.5$) and have abundant multi-wavelength data. Such objects are useful prototypes for the study of high redshift infrared luminous galaxies. However, these redshift surveys are still far from being a complete spectroscopic survey of all *IRAS* sources. Therefore, many ULIRGs remain undiscovered in FSC92.

More recent galaxy redshift surveys such as the Sloan Digital Sky Survey (SDSS, York et al. 2000), the 2dF Galaxy Redshift Survey (2dFGRS, Colless et al. 2001) and the 6dF Galaxy Survey (6dFGS, Jones et al. 2004) have provided redshifts for much larger samples of galaxies. These data will clearly be very useful for finding new ULIRGs in FSC92, which has been attempted by several studies (Cao et al. 2006; Goto 2005; Pasquali, Kauffmann, & Heckman 2005). However, Goto (2005) and Pasquali, Kauffmann, & Heckman (2005) cross-correlated the *IRAS* sources with the SDSS spectroscopic sample of galaxies using a circular matching tolerance instead of using a positional error ellipse of the *IRAS* sources. Cao et al. (2006) performed a similar cross-correlation using the formal positional error ellipses of the *IRAS* sources, but they used only the Second Data Release of SDSS.

In this paper we present a search for ULIRGs and HLIRGs from a cross-correlation of FSC92 with the most recent spectroscopic catalogues of galaxies in SDSS, 2dFGRS and 6dFGS, using positional matches in the *IRAS* error ellipses. The data used for the cross-correlation and the identification algorithm for ULIRGs and HLIRGs are presented in Section 2. Our main results are presented in Section 3, and are discussed in Section 4. We summarize and conclude

in Section 5. Throughout this paper, we assume that $H_0 = 70 \text{ km s}^{-1} \text{ Mpc}^{-1}$, $\Omega_0 = 0.3$ and $\Lambda = 0.7$.

2 IDENTIFICATION OF ULIRGS AND HLIRGS

2.1 The Samples and Cross-Correlation

We cross-correlated the *IRAS* sources in FSC92 with the spectroscopic sample of galaxies in the Fourth Data Release of SDSS (Adelman-McCarthy et al. 2005, hereafter SDSSDR4), the Final Data Release of 2dFGRS (Colless et al. 2001, hereafter 2dFGRSDRF) and the Second Data Release of 6dFGS (Jones et al. 2005, hereafter 6dFGSDR2). The FSC92 contains about 173,000 infrared sources with measured fluxes at 12 μm , 25 μm , 60 μm and 100 μm . The SDSSDR4 and the 2dFGRSDRF have a similar median depth of $\bar{z}=0.11$. The SDSSDR4 contains about 473,000 galaxies over 4,800 deg^2 , and the 2dFGRSDRF contains about 246,000 galaxies over 2,000 deg^2 . The 6dFGSDR2 which contains about 89,000 galaxies, covers a wider area ($\sim 13,600 \text{ deg}^2$) than the other surveys, but has a shallower median depth of $\bar{z}=0.05$.

The positional uncertainties of the *IRAS* sources are different for the in-scan direction and the cross-scan direction (typically 5'' for the in-scan direction and 16'' for the cross-scan direction, 1σ), and vary from source to source (1''–13'' for the in-scan direction, or minor axis of positional uncertainty ellipse and 3''–55'' for the cross-scan direction, or major axis of positional uncertainty ellipse, 1σ). The positional uncertainties of the optical identifications themselves are negligible in comparison. We use the positional uncertainty ellipse of FSC92 to find matching counterparts of the *IRAS* sources, instead of using a circular matching tolerance (to be discussed in Section 2.3). If a galaxy in a redshift survey lies within 3σ positional uncertainty ellipse of the *IRAS* source, we regard it a match. As a result of this matching, we find that 8382, 2091 and 10197 *IRAS* sources have optical counterparts in the SDSSDR4, 2dFGRSDRF and 6dFGSDR2, respectively. Some *IRAS* sources (615 for SDSSDR4, 201 for 2dFGRSDRF, and 91 for 6dFGSDR2) have more than two galaxies within 3σ error ellipse. In these cases, we computed the ‘‘Likelihood Ratio (LR)’’ (Sutherland & Saunders 1992, to be discussed in 2.3) of each association, and selected a more appropriate galaxy with the larger value of LR as an optical counterpart. In total, we compiled a list of 19,380 sources by collecting all matched sources from our disparate galaxy redshift surveys.

2.2 Selection Criteria

We used the following steps in order to identify bona-fide ULIRGs and HLIRGs from the list of all matched sources:

(i) For 19,380 sources in the list of all matched sources, we calculated the IR luminosities using the *IRAS* 60 μm fluxes and the redshifts of galaxies on the assumption that the ULIRGs and HLIRGs have M82 starburst Spectral Energy Distributions (SEDs). A substantial fraction of the *IRAS* sources have upper limit fluxes at 12 μm , 25 μm and 100 μm , so we use this single-band selection to obtain a less

³ The earlier version of this survey is the Bright Galaxy Survey (Soifer et al. 1986, 1987, 1989; Sanders et al. 1995).

Table 1. ULIRGs found in SDSSDR4, 2dFGRSDRF and 6dFGSDR2

FSC NAME	SDSS			6dFGS			2dFGRS			Final
	ID	z	zconf	ID	z	Q	ID	z	Q	
F00050–3259*							TGS434Z061	0.285	4	3
F00091–0738				g0011433–072207	0.118	4				2
F00091–3905*				g0011432–384913	0.254	3				2
F00095–5948*				g0011586–593133	0.235	4				2
F00184–3331*				g0020557–331428	0.239	3	TGS497Z156	0.239	4	2
F00256–0208				g0028143–015146	0.277	3				2
F00285–3140				g0030593–312445	0.218	2	TGS439Z175	0.217	4	3
F00318–3137*				g0034133–312118	0.285	4				2
F00335–2732							TGS206Z015	0.069	5	3
F00406–3127				g0043032–311050	0.343	1				2

Column descriptions: (1) The *IRAS* object name in the FSC92. Asterisks represent the sources that are identified as ULIRGs for the first time in this study; (2–4) The identification, the redshift, and the redshift confidence value in SDSSDR4; (5–7) The identification, the redshift, and the redshift quality parameter in 6dFGSDR2; (8–10) The identification, the redshift, and the redshift quality parameter in 2dFGRSDRF; (11) Finally accepted optical counterpart (1–SDSSDR4, 2–6dFGSDR2, 3–2dFGRSDRF).

Table 2. The *IRAS* data for the Final Sample of ULIRGs

FSC NAME	RA (J2000)	Dec (J2000)	12 μ m (Jy)	25 μ m (Jy)	60 μ m (Jy)	100 μ m (Jy)	Flux Qual
F00050–3259*	00 07 34.6	–32 43 03	0.066 (0.018)	0.144 (0.042)	0.222 (0.045)	0.758 (0.220)	1131
F00091–0738	00 11 43.3	–07 22 05	0.071 (0.020)	0.215 (0.054)	2.626 (0.184)	2.521 (0.202)	1232
F00091–3905*	00 11 42.3	–38 49 15	0.106 (0.030)	0.125 (0.038)	0.316 (0.047)	0.756 (0.227)	1131
F00095–5948*	00 11 58.8	–59 31 28	0.074 (0.014)	0.052 (0.010)	0.313 (0.034)	0.681 (0.123)	1132
F00184–3331*	00 20 57.7	–33 14 28	0.105 (0.028)	0.120 (0.035)	0.334 (0.047)	0.613 (0.141)	1132
F00256–0208	00 28 14.4	–01 51 47	0.108 (0.031)	0.323 (0.090)	0.602 (0.060)	0.611 (0.147)	1132
F00285–3140	00 31 03.0	–31 24 18	0.144 (0.042)	0.141 (0.041)	0.389 (0.051)	0.688 (0.199)	1132
F00318–3137*	00 34 16.0	–31 21 04	0.108 (0.030)	0.167 (0.048)	0.257 (0.062)	0.563 (0.158)	1132
F00335–2732	00 35 59.2	–27 15 42	0.144 (0.045)	0.632 (0.069)	4.294 (0.472)	3.207 (0.225)	1332
F00406–3127	00 43 03.0	–31 10 53	0.060 (0.016)	0.091 (0.025)	0.717 (0.057)	0.994 (0.169)	1132

Column descriptions: (1) The *IRAS* object name in the FSC92. Asterisks represent the sources that are identified as ULIRGs for the first time in this study; (2–3) Right ascension and declination; (4–7) The *IRAS* flux density (and its uncertainty) at 12 μ m, 25 μ m, 60 μ m and 100 μ m; (8) The *IRAS* flux density qualities at each band (1–upper limit, 2–moderate quality, 3–high quality).

heterogeneous final catalogue (to be discussed in Section 2.3).

(ii) We selected the sources for which their 60 μ m flux qualities are “high” or “moderate” (Moshir et al. 1992) in order to restrict our analysis to those sources with reliable 60 μ m detections⁴, obtaining 19,335 sources.

(iii) Of the 19,335 reliable sources, we classified 483 sources as ULIRG candidates (IR luminosities greater than $10^{12} L_{\odot}$), and classified 14 sources as HLIRG candidates (IR luminosities are greater than $10^{13} L_{\odot}$).

(iv) We then assessed the quality of the redshift for the ULIRG and HLIRG candidates. We required a redshift confidence of ≥ 0.65 for the SDSSDR4, a redshift quality of ≥ 3 for the 2dFGRSDRF, and a redshift quality is equal to 3 or 4 for the 6dFGSDR2. See each data release paper for the descriptions of these redshift quality parameters. On this ba-

sis, we secured 333 ULIRG and no HLIRG candidates with acceptable redshift qualities.

(v) We used the NASA/IPAC Extragalactic Database (NED) Near Position Search in order to reject chance coincidences of *IRAS* sources for which optical counterparts are already listed in the literature. We rejected 13 ULIRG candidates (two sources moved to a list of HLIRGs), and added 4 sources (to be discussed in Section 2.3). Our redshifts for these four are confirmed in the literature, although their redshift qualities do not satisfy our criteria. Finally we found 324 ULIRGs and 2 HLIRGs (the final two HLIRGs will be discussed in Section 4.3).

Table 1 lists the final sample of 324 ULIRGs with the names of the *IRAS* sources, the identifications of their optical counterparts, redshifts and redshift quality parameters in each galaxy redshift survey. In some cases, more than two disparate galaxies from different galaxy redshift surveys are located within an error ellipse of one *IRAS* source. Therefore, we present the flags indicating which galaxy has been adopted as the optical counterpart in the final column of Table 1. We present the *IRAS* FSC92 data in Table 2.

⁴ The flux measurements of high quality, moderate quality or upper limits are represented as number of 3, 2, 1 respectively in FSC92.

Table 3. The Final Sample of ULIRGs

FSC NAME	Final z	$\log L_{\text{IR}}$ (L_{\odot})	$\log(\text{LR})$	Class L/S
F00050–3259*	0.2855	12.12	0.5042	7/V
F00091–0738	0.1178	12.30	0.6345	7/IV
F00091–3905*	0.2535	12.14	0.5944	7/V
F00095–5948*	0.2349	12.06	0.6102	7/IV
F00184–3331*	0.2387	12.10	−0.1065	7/V
F00256–0208	0.2770	12.52	0.5735	5/IIIa
F00285–3140	0.2166	12.07	−0.9137	4/I
F00318–3137*	0.2846	12.18	0.3252	7/V
F00335–2732	0.0686	12.01	0.3877	7/IV
F00406–3127	0.3425	12.82	0.5803	7/V

Column descriptions: (1) The *IRAS* object name in the FSC92. Asterisks represent the sources that are identified as ULIRGs for the first time in this study; (2) Finally accepted redshift from galaxy redshift survey; (3) Infrared luminosity calculated in this study; (4) Likelihood ratio; (5) Morphological class using Lawrence classification (L) and Surace classification (S). See the description in the end of this section.

Adopted redshifts, IR luminosities, log (LR) and morphological classes (to be discussed at the end of this section) are listed in Table 3.

Figure 1 shows a sample of $3' \times 3'$ finding charts (left hand panels) for the final sample of ULIRGs extracted from the SDSS *gri* composite images or the SuperCOSMOS scans of r_F survey plates. The contour plot for each ULIRG using the SDSS *r*-band images or the SuperCOSMOS r_F images is also presented in Figure 1 (right hand panels). Using Figure 1, we classify the interaction types of the ULIRGs in the final sample. The ULIRGs are classified according to the modified version of the interaction classification schemes of Lawrence et al. (1989, hereafter Lawrence classification) (see, e.g., Farrah et al. 2001) and of Surace (1998, hereafter Surace classification) (see, e.g., Veilleux, Kim & Sanders 2002), as are summarised in Table 4. The results of the classification are given in the last column of Table 3. The complete versions of Table 1, Table 2, Table 3 and Figure 1 are available only in the electronic issue. A brief discussion of some ULIRGs is given in Appendix A that is available in the electronic issue.

2.3 Reliability of Identifications

A variety of definitions of ULIRGs have been used in the literature, and depend on the minimum luminosity, the adopted spectral energy distributions and the cosmology ($L_{8-1000} \geq 10^{12} L_{\odot}$ with $H_0 = 75 \text{ km s}^{-1} \text{ Mpc}^{-1}$ and $q_0 = 0.0$ for Sanders & Mirabel 1996, Kim & Sanders 1998, and Goto 2005; $L_{60} \geq 10^{10.77} L_{\odot}$ with $H_0 = 100 \text{ km s}^{-1} \text{ Mpc}^{-1}$ and $q_0 = 0.5$ for Clements et al. 1996a; $L_{60} \geq 10^{12} L_{\odot}$ with $H_0 = 50 \text{ km s}^{-1} \text{ Mpc}^{-1}$ and $\Omega = 1$ for Lawrence et al. 1999). In order to check the reliability of our selection criteria of ULIRGs, we compiled 636 known ULIRGs taken mostly from wide area survey data (Leech et al. 1994; Clowes et al. 1995; Murphy et al. 1996; Clements et al. 1996a; Duc, Mirabel & Maza 1997; Kim & Sanders 1998; Clements, Saunders & McMahon

1999; Lawrence et al. 1999; Rigopoulou et al. 1999; Stanford et al. 2000; Sanders et al. 2003; Goto 2005; Cao et al. 2006). We then applied the same procedure given in Section 2.2 to select ULIRGs in this sample of known ULIRGs. Of these known ULIRGs from the literature, we found 291 reliable sources in step (ii) of Section 2.2. A total of 345 known ULIRGs were not found since they were neither observed in the redshift surveys of this study nor included in FSC92. After the final identification step in Section 2.2, we found 131 known ULIRGs in our final sample of ULIRGs, and failed to find a total of 160 ULIRGs. The reasons our having missed these 160 known ULIRGs are categorised as follows:

(i) **Different redshifts** (F00415–0737, F01031–2255, F01082–2452, F03014–2026, F03193–2224, F03448–2628, F08509–1504, F10122+4943, F20087–0308, F20109–3003, F20175–4756, F23515–2917): For the sources in this category, the redshifts used in this study are different to (and almost always much lower than) those in the literature. Therefore, the IR luminosities calculated in this study are not large enough to be selected as ULIRGs in this study. Some sources have high redshift qualities (F00415–0737, F08509–1504, F10122+4943, F20109–3003), while the redshift qualities for the others are low. The redshift of F01031–2255 used in this study is larger than that in the literature, but it is not included in the final sample of ULIRGs due to its low redshift quality.

(ii) **Different optical counterpart galaxies** (F03202–0001, F08007+3928, F09346+3911, F12527–0306, F14390+6209, F14475+0155, F14546+0338, F15182+3023, F21368+1006, F22011+0017, F23051–0100): The optical counterpart galaxies of these *IRAS* sources in this study are different from the galaxies in the literature, as are their redshifts.

(iii) **Different 60 μm fluxes** (F00444–1803, F09320+6134, F11087+5351, F14170+4545, F14351–1954, F14575+3256, F18520–5048): The IR luminosities of these sources are not greater than $10^{12} L_{\odot}$ since the 60 μm fluxes of these sources used in this study (from FSC92) are lower than the fluxes used in the literature (mostly from PSC).

(iv) **Marginal ULIRGs** (F12495–3414, F13156+0435, F14378–2604, F22509–0040): Since the L_{60} luminosities of all four sources are slightly less than $10^{12} L_{\odot}$, they were classified as *further marginal/possible ULIRGs* in Lawrence et al. (1999). Similarly, their IR luminosities calculated in this study are in the range of $10^{11.84} - 10^{11.95} L_{\odot}$, therefore they are not classified as ULIRGs in this study.

(v) **Low qualities of redshifts** (F00406–3127, F10026–0022, F14207–2002, F14485–2434, F22123–2025): These sources satisfy the selection criteria up to step (iii) of Section 2.2. However, they fail to satisfy the criteria in step (iv) of Section 2.2 due to their low redshift qualities. Although the redshift qualities of F00406–3127, F14485–2434 and F22123–2025 are low, these redshifts are same as those quoted in the literature. Therefore we include these three sources in the final sample of ULIRGs. F14207–2002 is not a known ULIRG, but its redshift in this study is same as that of Allen et al. (1991). Therefore we also include F14207–2002 in the final sample of ULIRGs. However, F10026–0022 was identified as a ULIRG in Goto (2005) using the same SDSS data with low quality of redshift as in

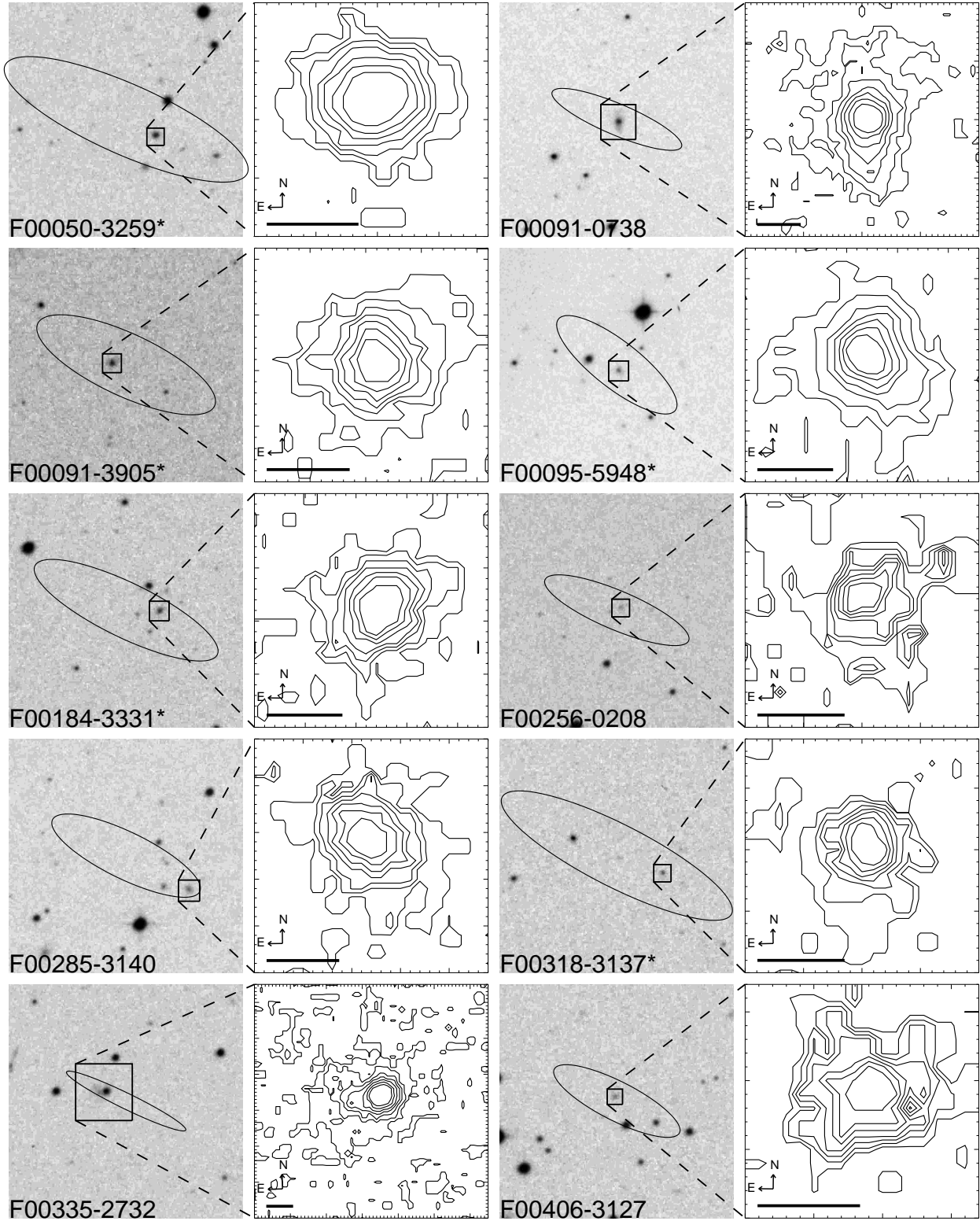


Figure 1. The $3' \times 3'$ finding charts (left in each panel) and contour plots (right in each panel) of 324 ULIRGs identified in this study. The finding charts centred on *IRAS* source positions are extracted from the SDSS *gri* composite images or the SuperCOSMOS scans of r_F survey plates. North is up, and the East is to the left. The ellipse represents 3σ *IRAS* positional uncertainty. The optical counterpart in the redshift surveys is marked by square indicating the size, orientation and location of the contour plot in the finding chart. The *IRAS* object names are presented in the bottom left corner, and asterisks represent the newly identified ULIRGs in this study. The contour plots centred on optical counterparts represent the intensities of ULIRGs in the SDSS *r*-band images or the SuperCOSMOS r_F images. The size of each contour plot is $40 \text{ kpc} \times 40 \text{ kpc}$. The contour levels increase from the sky level (I_{sky}) to the peak value (I_{max}) by factors $10^{(I_{\text{max}} - I_{\text{sky}})/8}$. The orientation is indicated by the arrows and the thick, horizontal bar represents 5 arcsec in each contour plot.

Table 4. The interaction classification scheme of ULIRGs used in this study

Scheme	Class	Description
Lawrence classification	0	Isolated source with no signs of interaction or merging
	1	Source with a faint companion (2~4 mag fainter than the source) in the range of 40~200 kpc
	2	Source with a bright companion (less than 2 mag fainter than the source) in the range of 40~200 kpc
	3	Source with a faint companion less than 40 kpc
	4	Source with a bright companion less than 40 kpc
	5	Source interacting with a companion and showing signs of interaction
	6	Merger/More than two nuclei in common envelope
7	Merger/Single nuclei in common envelope	
Surace classification	I	First approach – Unperturbed and separated galaxies with no signs of interaction or merging
	II	First contact – Overlapped disks but no strong bars and tidal tails
	IIIa	Pre-merger a – Two recognisable nuclei with strong signs of interaction and separated more than 10 kpc
	IIIb	Pre-merger b – Two recognisable nuclei with strong signs of interaction and separated less than 10 kpc
	IV	Merger – Only one nucleus seen with strong tidal features
V	Old merger – No direct signs of tidal features but disturbed central morphology	

this study. Therefore we reject it from the final catalogue of ULIRGs.

(vi) **Underluminous ULIRGs** (F00090–0054, F08112+3039, F08322+3609, F09045+3943, F16134+2919, F21341–0033): These sources are the FIRST-FSC sample of Stanford et al. (2000). They did not use a strict minimum infrared luminosity to identify ULIRGs. The far-infrared (FIR) luminosities for these sources in Stanford et al. (2000) are in the range of $10^{11.27} - 10^{11.85} L_{\odot}$ which is similar to the minimum FIR luminosity of ULIRGs in Sanders & Mirabel (1996). Similarly, these sources are not selected as ULIRGs in this study due to our low estimates for their IR luminosities ($10^{11.44} - 10^{11.99} L_{\odot}$).

(vii) **Different SEDs** (F21219–1757): This source was classified as a ULIRG in Kim & Sanders (1998) with $\log(L_{ir}/L_{\odot})=12.06$. However, the IR luminosity calculated in this study is $\log(L_{ir}/L_{\odot})=11.86$ which does not satisfy the ULIRGs criteria, although the redshift and *IRAS* flux densities used in this study are same as those in Kim & Sanders (1998). This is because we used M82 starburst SED to calculate the IR luminosity which may not be appropriate for low luminosity QSOs such as this. If we use AGN dominated SED⁵ of NGC 1068 to calculate the IR luminosity for this source, we obtain the IR luminosity of $\log(L_{ir}/L_{\odot})=12.14$, satisfying the ULIRGs criteria.

(viii) **Using upper limit flux** (115 objects): These sources were classified as ULIRGs in Goto (2005) and Cao et al. (2006). Although most *IRAS* galaxies have upper limit fluxes at 12 μ m and 25 μ m (to be discussed in the end of this section), Goto (2005) calculated the IR luminosities of *IRAS* sources by treating the flux upper limits as detections. Similarly, three sources for which 100 μ m flux densities are “upper limits” were found to be ULIRGs in Cao et al. (2006) by assuming the 100 μ m upper limit is obtained. These calculations can clearly result in overestimates for the IR luminosities of *IRAS* galaxies. These sources are

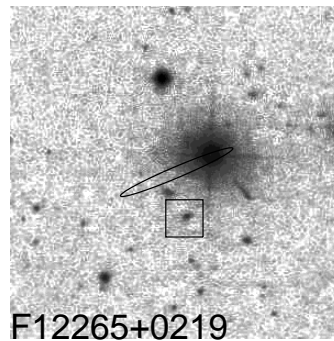


Figure 2. The 2'×2' finding chart of F12265+0219 extracted from the SDSS *gri* composite image. The finding chart centred on *IRAS* source position. North is up and East is to the left. The ellipse represents 3 σ positional uncertainty, and the square denotes the optical counterpart found in Goto (2005), SDSS J122907.3+020246. The star like object within the ellipse is 3C 273.

not selected in our study as ULIRGs due to their low IR luminosities of $10^{10.60} - 10^{11.99} L_{\odot}$.

In summary, all 160 known ULIRGs that are not identified in this study have appropriate reasons not to be selected as ULIRGs except for only one source (F21219–1757). Therefore we conclude that our ULIRGs selection criteria are reliable and good enough to identify nearly all known ULIRGs.

Goto (2005) performed a cross-correlation of FSC92 with the spectroscopic catalogues of galaxies in the SDSS Third Data Release (SDSSDR3), and identified 178 ULIRGs and 3 HLIRGs. Since the SDSSDR4, which we used for our cross-correlation in this study, contains galaxies of SDSSDR3, we can compare our identification procedure of ULIRGs and HLIRGs with that of Goto (2005). Firstly, we accept the correlation if a galaxy in SDSSDR4 lies within 3 σ positional uncertainty ellipse of the *IRAS* source, while Goto (2005) treats a neighbouring optical galaxy as a match if the galaxy in SDSSDR3 lies within 20 arcsec of the *IRAS* source without regard to the *IRAS* error ellipse. This can cause many problems. For example,

⁵ If we use AGN dominated SED of NGC 1068 to calculate the IR luminosities for ‘Warm’ ULIRGs ($f_{25}/f_{60} > 0.2$) in the final sample, the IR luminosities for those sources will be increased by 82 per cent.

SDSS J122907.3+020246 was identified as a HLIRG in Goto (2005). In Figure 2, we present the SDSS *gri* composite image of F12265+0219, which was regarded as the *IRAS* counterpart of SDSS J122907.3+020246 in Goto (2005). It is seen that SDSS J122907.3+020246 lies outside the 3σ error ellipse and a bright star-like object lies within the ellipse. The star-like object within the ellipse is the famous quasar 3C 273, which is known to be associated with F12265+0219. Since 3C 273 was not included in the spectroscopic targets of the SDSS and Goto (2005) used circular matching tolerance of 20 arcsec, the mismatch between F12265+0219 and SDSS J122907.3+020246 was included in his sample. Our cross-correlation based on the positional error ellipse, and the NED Near Position Search in step (v) of Section 2.2 help to avoid this kind of mismatching. Secondly, there is a difference in the calculation of infrared luminosity between Goto (2005) and this study. The former used the same function as used by Kim & Sanders (1998) for the calculation of IR luminosity using *IRAS* flux directly from FSC92. However, a significant fraction (81 per cent of “high” or “moderate” $60\ \mu\text{m}$ sources for f_{12} fluxes⁶ and 74 per cent for f_{25} fluxes) of the *IRAS* sources only have upper limits for f_{12} and f_{25} fluxes. Therefore, assuming upper limits are obtained for the measurements at f_{12} and f_{25} in calculating the IR luminosity can lead to overestimates of the IR luminosity, although the uncertainty in the IR luminosity is only a few per cent (Kim & Sanders 1998).

2.4 Reliability and Completeness of the final sample

A final sample of ULIRGs selected by cross-correlation based on the position alone may contain spurious sources due to the chance presence of a galaxy within the *IRAS* 3σ ellipse. In order to estimate the probability of the “true” association between *IRAS* sources and the optical counterparts, we compute likelihood ratio (Sutherland & Saunders 1992) for each association. The likelihood ratio defined by the ratio of the probability of a true association to that of a chance association is⁷

$$\text{LR} = \frac{Q(\leq m) \exp(-r^2/2)}{2\pi\sigma_1\sigma_2 n(\leq m)}, \quad (1)$$

where $n(\leq m)$ is the local surface density of objects brighter than the candidate. The “normalised distance” r is given by

$$r^2 = \left(\frac{d_1}{\sigma_1}\right)^2 + \left(\frac{d_2}{\sigma_2}\right)^2, \quad (2)$$

where the d_1 , d_2 are the positional differences along the two axes of an error ellipse for an *IRAS* source, and σ_1 , σ_2 are the lengths of these axes. Since the positional uncertainties of galaxies in SDSS, 2dFGRS, and 6dFGS are negligible compared with those of *IRAS* sources, we define σ as the length of the error axes of the *IRAS* sources. $Q(\leq m)$ is a multiplicative factor which is the a priori probability that a “true” optical counterpart brighter than the magnitude limit exists in the association, and for simplicity we set $Q = 1$ in this study.

⁶ The quantities f_{12} , f_{25} , f_{60} , and f_{100} represent the *IRAS* flux densities in Jy at $12\ \mu\text{m}$, $25\ \mu\text{m}$, $60\ \mu\text{m}$, and $100\ \mu\text{m}$, respectively.

⁷ We assume that a positional error of *IRAS* source is a Gaussian.

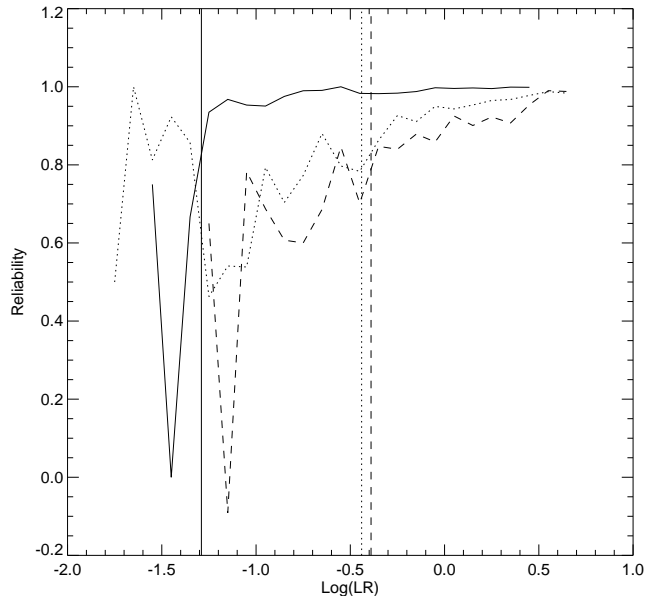


Figure 3. Reliability of our cross-correlation for SDSSDR4 (dotted line), 2dFGRSDF (dashed line) and 6dFGSDR2 (solid line) as a function of LR. The vertical lines represent the critical LR values of reliable identification for each redshift survey data - above the critical LR values, the reliabilities are $\geq 80\%$.

We compute $n(\leq m)$ using photometric sample of galaxies within 3σ error ellipse,

$$n(\leq m) = \frac{N(\leq m)}{9\pi\sigma_1\sigma_2} \quad (3)$$

where $N(\leq m)$ represents the number of galaxies of which magnitudes⁸ are less than or equal to that of a candidate. We then obtain the likelihood ratio for our sample

$$\text{LR} = \frac{9 \exp(-r^2/2)}{2N(\leq m)}. \quad (4)$$

We compute LR values for all 19,380 sources in the list of all matched sources of Section 2.1 using the photometric sample of galaxies in each redshift survey. In order to calculate the reliability of association using the LR values, we perform random associations by offsetting the *IRAS* source positions by $\approx 30'$, and recompute LR values for each random association following Lonsdale et al. (1998) and Masci et al. (2001). Using the distribution of LR values for true associations and random associations, the reliability of each association with a given LR is defined by

$$R(\text{LR}) = 1 - \frac{N_{\text{random}}(\text{LR})}{N_{\text{true}}(\text{LR})}, \quad (5)$$

where $N_{\text{true}}(\text{LR})$ and $N_{\text{random}}(\text{LR})$ are the number of true and random associations with a given LR. In Figure 3, we present the reliability of our cross-correlation for each redshift survey as a function of LR. Above $\log(\text{LR}) \sim -0.44$ (SDSSDR4), -0.39 (2dFGRSDF), -1.29 (6dFGSDR2), the reliabilities are $\geq 80\%$. We show the LR distribution of our

⁸ We use SDSS Petrosian r-band magnitude for the galaxies in SDSSDR4, and b_j band magnitude for the galaxies in 2dFGRSDF and 6dFGSDR2.

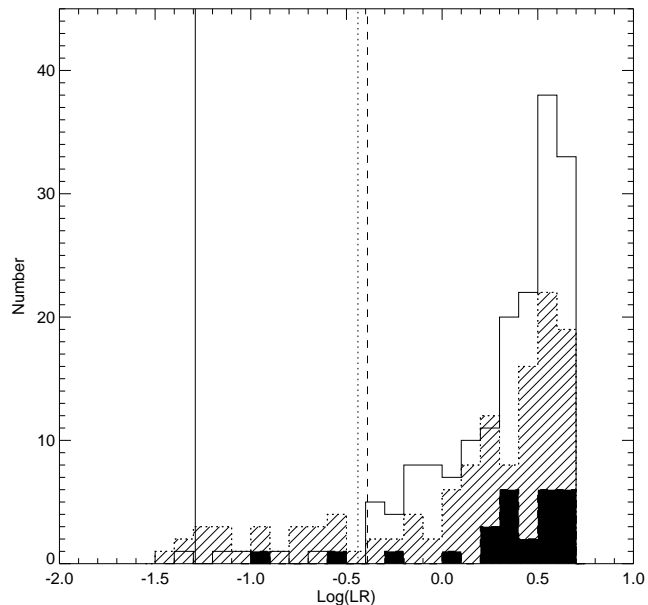


Figure 4. Distribution of LR values for the final sample of 324 ULIRGs found in SDSSDR4 (shaded region), 2dFGRSDF (filled region), and 6dFGSDR2 (solid line). The vertical lines represent the critical LR values of reliable identification (the reliability of $\sim 80\%$) as shown in Figure 3.

ULIRG sample in Figure 4 along with critical LR values of reliable identification for each redshift survey. If we apply the critical LR values of 80% reliability, then 24 out of 126 (SDSSDR4), 2 out of 27 (2dFGRSDF), and 1 out of 171 (6dFGSDR2) ULIRGs can be rejected from a final sample of ULIRGs.

The reliability of our LR-based identifications is confirmed by the NED Near Position Search in Section 2.2. Of the 11 objects that were rejected from our final sample of ULIRGs because the optical association differs from that in NED, eight have lower LR values than the critical values. Although three objects have larger LR values than the critical values, there are more appropriate galaxies in NED (the larger value of LR) that would result in the galaxies not being ULIRGs.

The spectroscopic target selection in a redshift survey introduces incompleteness into our final sample of ULIRGs. Since the target selection functions differ in our three redshift surveys (a short discussion is presented in Section 4.1) and are beyond the scope of this paper, we only estimate the incompleteness originated from this study. Therefore, we measure the completeness relative to all FSC92 ULIRGs that are identified in these surveys, and *not* for example relative to a volume-limited ULIRG survey or to FSC92 as a whole.

There are three factors which make our sample incomplete. Firstly, since we used 3σ error ellipse for our cross-correlation, some ULIRGs outside 3σ error ellipse might be missed. If we assume an error ellipse to be a Gaussian distribution, the incompleteness originated from this term would be about 1 per cent. Secondly, some ULIRGs for which redshift qualities are unreliable (step (iv) in Section 2.2) are rejected, although their redshifts are not wrong. Thirdly, when more than two galaxies including a known optical counter-

part galaxy are within the error ellipse of one *IRAS* source, the wrong galaxy may be selected as the optical counterpart of the *IRAS* source. In order to quantify the incompleteness introduced by those factors, we compute the ratio of ULIRGs that are surveyed in SDSSDR4, 2dFGRSDF and 6dFGSDR2 to those that are missed from our final sample of ULIRGs using previously known ULIRGs. Of the 636 known ULIRGs in Section 2.3, we consider only the 140 known ULIRGs that are expected to be found in this study. This sample consists of ULIRGs that are located within the redshift survey region and are found in FSC92. Additionally, their IR luminosities calculated using our method are greater than $10^{12} L_{\odot}$. In the result of identification procedure in Section 2.1 and 2.2, 133 ULIRGs are found in our final sample of ULIRGs, and 7 ULIRGs are missed.

Of the 7 missed ULIRGs, three *IRAS* sources (F03202-0001, F14546+0338 and F22011+0017) have more than two galaxies including a known optical counterpart within their error ellipses. Our selection procedure is to choose the most likely counterpart (i.e. the galaxy with the larger value of LR), but this selects different galaxies to the known optical counterparts for these three *IRAS* sources. Therefore, the incompleteness introduced by our selection using LR values among several counterpart candidates is about 2.1 per cent (3 out of 140), although all the optical counterparts that we select are brighter or closer to the *IRAS* position than the known optical counterparts. In addition, one ULIRG (F09111-1007) is missed, because the optical counterpart in 6dFGSDR2 is outside 3σ error ellipse, although the association is already confirmed in the literature. Three ULIRGs (F00406-3127, F14485-2434, and F22123-2025) are missed because of their low redshift qualities as shown in Section 2.3, although the redshifts quoted in the redshift surveys are same as those in the literature. Therefore, the incompleteness introduced by our cross-correlation algorithm using 3σ error ellipse is about 0.7 per cent (1 out of 140), and the incompleteness introduced by our selection using the redshift quality parameter in the step (iv) of Section 2.2 is about 2.1 per cent (3 out of 140). In total, the incompleteness of the final sample of ULIRGs originated from this study is about 5 per cent (7 out of 140).

3 RESULTS

We have found 324 ULIRGs (126 in SDSSDR4, 27 in 2dFGRSDF, and 171 in 6dFGSDR2), 190 of which are newly discovered. We have therefore increased the number of known ULIRGs by about 30 per cent.

In Figure 5, we present the redshift distribution for the final sample of 324 ULIRGs identified in this study, and compare it to that of the 636 previously known ULIRGs. The redshifts in our final sample run from $z=0.037$ to $z=0.517$ and the median value is $\bar{z}=0.223$, which is larger than the median redshift $\bar{z}=0.184$ of the 636 previously known ULIRGs.

In Figure 6, we plot the IR luminosities of the ULIRGs identified in this study against their redshifts. In the upper and right panel, we present the redshift and luminosity distribution of ULIRGs found in each redshift survey, respectively. The ULIRGs identified in SDSSDR4 are found from low z to high z and from low luminosity to high luminosity

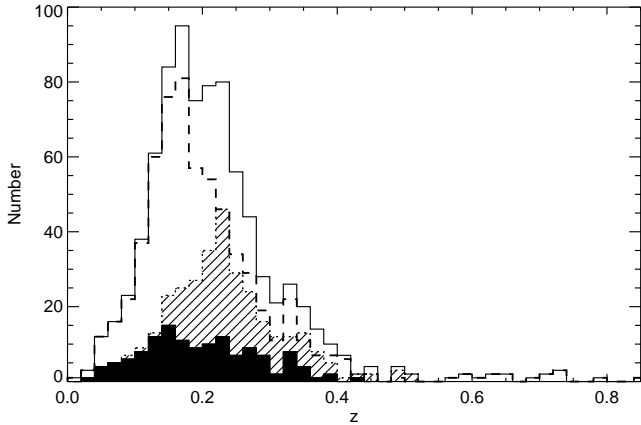


Figure 5. Redshift distribution of the 324 ULIRGs identified in this study (shaded region) compared to the 636 known ULIRGs (dashed lines), 134 known ULIRGs in the final sample in this study (filled region) and known ULIRGs plus all identified ULIRGs in this study (solid lines).

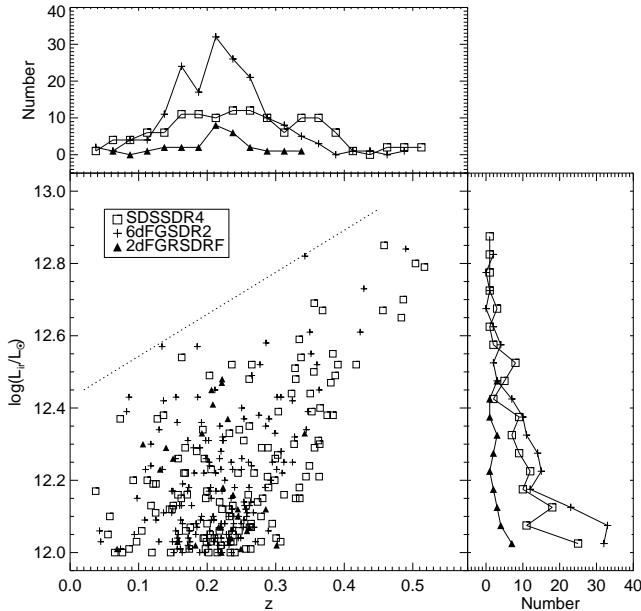


Figure 6. The IR luminosity of identified ULIRGs in this study versus redshift. The ULIRGs from the SDSSDR4, 2dFGRSDRF and 6dFGSDR2 are represented by squares, triangles, and pluses, respectively. In the upper and right panel, the redshift and luminosity distribution of ULIRGs found in each redshift survey are shown, respectively.

($\sim 10^{12.85} L_{\odot}$). The ULIRGs in 6dFGSDR2 show similar distribution with those in SDSSDR4, although median redshift of galaxies in 6dFGSDR2 is smaller than that of galaxies in SDSSDR4. In contrast, in spite of relatively larger median redshift of galaxies in 2dFGRSDRF compared to that of 6dFGSDR2, no ULIRGs in 2dFGRSDRF are found beyond $z \sim 0.35$. This might be due to the different selection criteria for spectroscopic targets (see each data release paper for more detail). Figure 6 shows that the upper envelope (shown by a dotted line) increases from $\log(L_{ir}/L_{\odot}) = 12.45$ to 12.95 as redshift increases. The lower envelope is due to the survey detection limit.

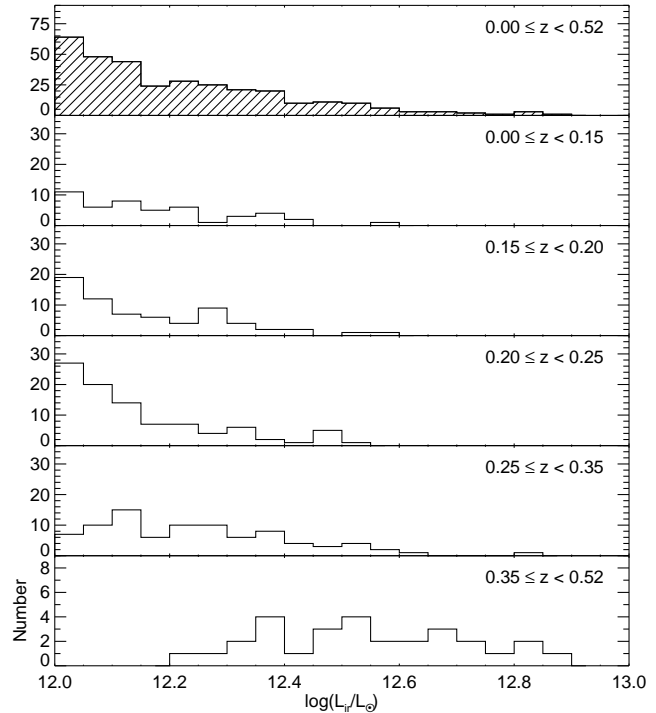


Figure 7. The luminosity distribution for the final sample of 324 ULIRGs is plotted in the top panel. Below this panel, the luminosity distributions of ULIRGs in the redshift ranges $0.00 \leq z < 0.15$, $0.15 \leq z < 0.2$, $0.2 \leq z < 0.25$, $0.25 \leq z < 0.35$, and $0.35 \leq z$ are shown.

The luminosity distribution of the final sample is plotted in the Figure 7. For the final sample of ULIRGs (top panel), there are fewer ULIRGs at high luminosities than at low luminosities. The median luminosity value is $10^{12.17} L_{\odot}$. Two interesting features are seen in the luminosity variation with redshift in Figure 7. Firstly, the number ratio of low luminous ULIRGs ($L_{ir} < 10^{12.2} L_{\odot}$) to all ULIRGs in redshift bin increases with redshift up to $z=0.25$ (due to the detection limit seen in Figure 6, there are few low luminous ULIRGs beyond $z=0.25$). Secondly, no ULIRGs that have IR luminosities of $\log(L_{ir}/L_{\odot}) > 12.60$ are found in the lower redshift ($z < 0.25$). This is almost certainly due to the evolving luminosity function. A calculation of the evolving luminosity function is beyond the scope of this paper.

4 DISCUSSION

4.1 Comparison of ULIRG subsamples

Since we use three different redshift survey data to search for ULIRGs, different target selection functions in each redshift survey make our final sample of ULIRGs inhomogeneous. The majority of spectroscopic targets in each redshift survey are selected from magnitude limited samples⁹,

⁹ The primary sample ($\sim 70\%$) of 6dFGS are galaxies with $K_{tot} < 12.75$ and one additional sample is optically selected galaxies with $b_J < 16.75$ ($\sim 5\%$). Most spectroscopic targets of 2dFGRS are galaxies with $b_J < 19.45$, and the main galaxy sample

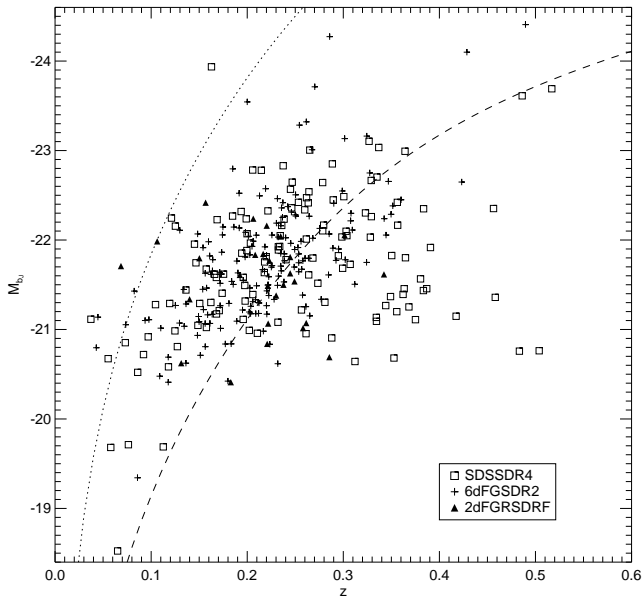


Figure 8. Absolute b_J magnitude of ULIRG subsamples against redshift. The ULIRGs from the SDSSDR4, 2dFGRS and 6dFGS2 are represented by squares, triangles, and pluses, respectively. The dotted and dashed line indicate the b_J magnitude limit of 6dFGS2 and 2dFGRS, respectively.

but some additional spectroscopic targets are included depending on the redshift survey. In order to see the effects of the magnitude limit of each survey on our ULIRG subsamples, we plot the absolute b_J magnitude against redshift of ULIRG subsamples in Figure 8. A transformation from SDSS photometry to b_J magnitude, and k -correction is done following Norberg et al. (2002). Since the majority of the spectroscopic targets in 6dFGS are K -band selected, most ULIRGs found in 6dFGS2 are fainter than the b_J magnitude limit ($b_J = 16.75$) shown by the dotted line. The majority of ULIRGs found in 2dFGRS are above the magnitude limit ($b_J = 19.45$). The b_J magnitude limit for the spectroscopic sample of SDSSDR4 is not clearly defined since the main spectroscopic sample of galaxies are Petrosian r -band selected sample. However, b_J magnitude limit for the main galaxy sample of SDSSDR4 is similar to that of 2dFGRS, and most galaxies fainter than the b_J magnitude limit are “Luminous Red Galaxies” (see Adelman-McCarthy et al. 2005 for more detail). It appears that a significant fraction (37%) of ULIRGs found in SDSSDR4 are fainter than the magnitude limit of 2dFGRS, implying that they are Luminous Red Galaxies.

In order to compare the infrared properties of our ULIRG subsamples associated with each redshift survey, we plot the infrared colour of $\log(f_{25}/f_{60})$ against $\log(f_{60}/f_{100})$ (a detailed discussion on the infrared colours of ULIRGs will be given in Section 4.2). Although the majority of ULIRGs in the range of $\log(f_{60}/f_{100}) < -0.4$ or in the range of $\log(f_{25}/f_{60}) > -0.7$ are *IRAS* sources with flux quality of 1 at $100\mu\text{m}$ or at $25\mu\text{m}$ (see Figure 11 and 12), there are no

of SDSS are galaxies with Petrosian r -band magnitudes brighter than $r=17.77$.

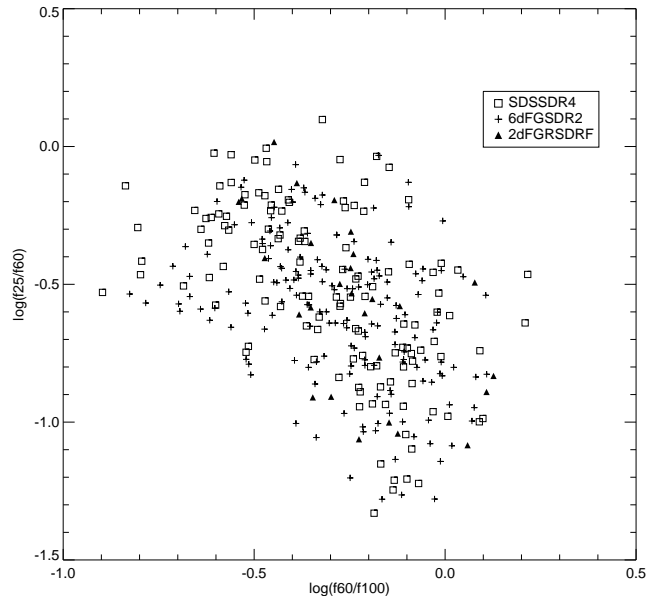


Figure 9. Infrared colour-colour diagram. $\log(f_{25}/f_{60})$ is plotted against $\log(f_{60}/f_{100})$ for the ULIRG subsamples. The ULIRGs from the SDSSDR4, 2dFGRS and 6dFGS2 are represented by squares, triangles, and pluses, respectively.

striking differences in infrared colours among the ULIRG subsamples associated with each redshift survey.

In conclusion, the sample of ULIRGs found in the three redshift surveys are not a simple magnitude limited sample due to the diverse target selection functions of each redshift survey.

4.2 Infrared Colours

Infrared colours such as $\log(f_{12}/f_{60})$, $\log(f_{25}/f_{60})$ and $\log(f_{60}/f_{100})$ have long been used for classifying infrared sources. Infrared-bright stars have SEDs peaking typically around $12\mu\text{m}$, and can be distinguished from galaxies using the colour of $\log(f_{12}/f_{60})$ (see, e.g., Cohen et al. 1987). In addition, $\log(f_{25}/f_{60})$ has been used to classify ULIRGs into ‘Warm’ and ‘Cool’ systems. It has been suggested that ULIRG may evolve from ‘Cool’ system to ‘Warm’ system (Sanders et al. 1988b; Veilleux, Kim & Sanders 2002). Soifer & Neugebauer (1991) showed that for luminous infrared galaxies including ULIRGs in the *IRAS* Bright Galaxy Survey, the mean $\log(f_{60}/f_{100})$ colour increases with increasing IR luminosity.

We present the IR luminosity against infrared colour of $\log(f_{12}/f_{60})$ in Figure 10, against $\log(f_{25}/f_{60})$ in Figure 11, and against $\log(f_{60}/f_{100})$ in Figure 12 for the final sample of 324 ULIRGs. The infrared-bright stars are known to have $\log(f_{12}/f_{60}) > 0$ (see, e.g., Kim & Sanders 1998). All ULIRGs in the final sample have infrared colours of $\log(f_{12}/f_{60}) < 0$.

In Figure 11, we plotted the boundary lines for the classification of normal galaxies, Seyfert 2 galaxies, and QSOs suggested by Neff & Hutchings (1992). If we restrict our attention to the ULIRGs with flux qualities of 2 or 3 (filled circles), the number ratio of these objects is $N(\text{Galaxy}) : N(\text{Sy2}) : N(\text{QSO}) = 32 : 7 : 29$. If we use the classification

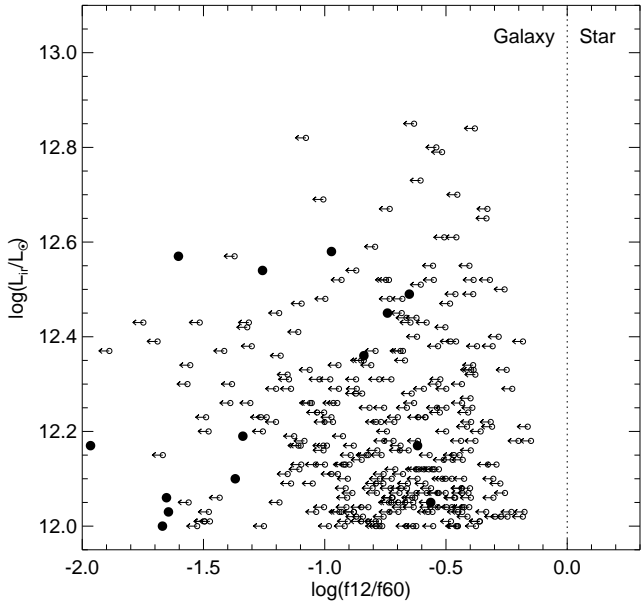


Figure 10. The infrared luminosity against the infrared colour $\log(f_{12}/f_{60})$ for the final sample of 324 ULIRGs in this study. The ULIRGs with flux upper limits at $12\ \mu\text{m}$ are represented by open circles with arrows indicating the sense of the limit, and the ULIRGs with high or moderate flux qualities are represented by filled circles. The dotted line represents the boundary between galaxies and stars.

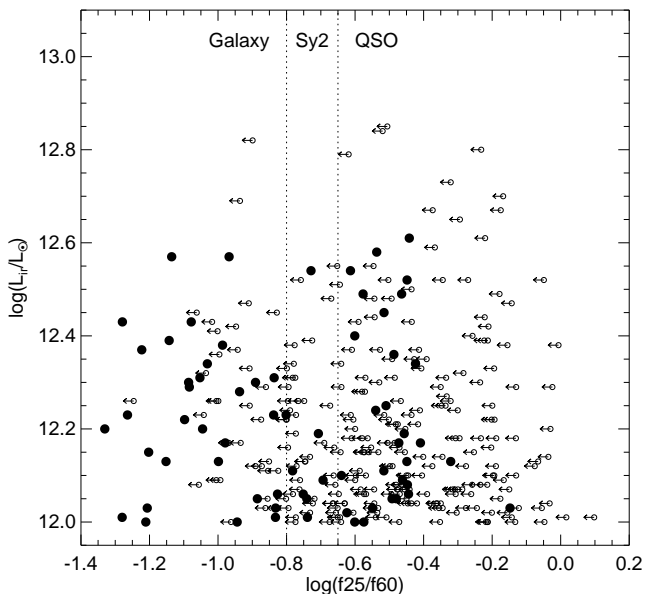


Figure 11. As Figure 10, except using the infrared colour $\log(f_{25}/f_{60})$. The open circles and arrows represent the ULIRGs which have upper limits at $25\ \mu\text{m}$, and the filled circles denote the ULIRGs which have high or moderate flux qualities at $25\ \mu\text{m}$. The dotted lines represent the boundaries among normal galaxies, Seyfert 2 galaxies, and QSOs.

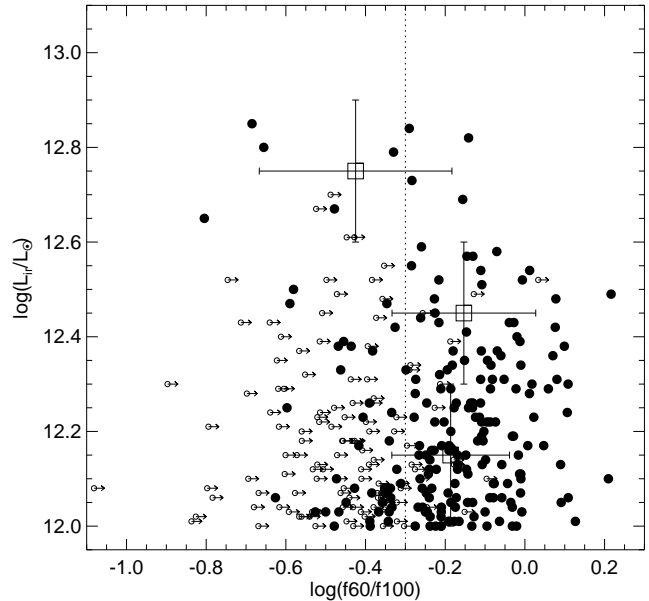


Figure 12. As Figure 10, except using the infrared colour $\log(f_{60}/f_{100})$. The ULIRGs with flux upper limits at $100\ \mu\text{m}$ are represented by open circles with arrows indicating the sense of the limit, and the ULIRGs with high or moderate flux qualities are represented as filled circles. The open squares are at the mean colour and the central luminosity of ULIRGs in the three luminosity bins ($12.0 \leq \log(L_{ir}/L_{\odot}) < 12.3$, $12.3 \leq \log(L_{ir}/L_{\odot}) < 12.6$, and $12.6 \leq \log(L_{ir}/L_{\odot}) < 12.9$). The vertical errorbars define the limiting luminosities of the bins, and the horizontal errorbars represent standard deviation of $\log(f_{60}/f_{100})$ colours in each bin. The dotted line represents the selection criteria ($\log(f_{60}/f_{100}) > -0.3$) of 1 Jy sample of ULIRGs (Kim & Sanders 1998).

scheme of ‘Warm’ ULIRGs ($f_{25}/f_{60} > 0.2$, or $\log(f_{25}/f_{60}) > -0.7$) and ‘Cool’ ULIRGs ($f_{25}/f_{60} < 0.2$, or $\log(f_{25}/f_{60}) < -0.7$) suggested by Sanders et al. (1988b), the number ratio for the sample becomes $N(\text{Cool}) : N(\text{Warm}) = 38 : 30$. This ratio is much smaller than that of 1 Jy sample ($N(\text{Cool}) : N(\text{Warm}) = 90 : 25$, Kim & Sanders 1998). This difference might be related to the different selection criteria for ULIRGs, but is likely to be strongly affected by the exclusion of ULIRGs which have upper limit flux at $25\ \mu\text{m}$.

In Figure 12, the $\log(f_{60}/f_{100})$ colours of ULIRGs with flux quality of 2 or 3, range from -0.80 to $+0.22$ and have a mean of -0.19 . This mean value is low compared to those of other ULIRG samples (see, e.g., Kim & Sanders 1998 and references therein). In addition, 21 per cent (42 out of 203) of ULIRGs with flux quality of 2 or 3, have colours of $\log(f_{60}/f_{100})$ less than -0.3 , while no ULIRGs in 1 Jy sample have colours of $\log(f_{60}/f_{100})$ less than -0.3 due to their selection criteria ($\log(f_{60}/f_{100}) > -0.3$) of ULIRGs (Kim & Sanders 1998). We plotted the mean colours in each luminosity bin by open squares to investigate any dependence of the colour on the IR luminosity. It appears that there are no significant IR luminosity dependence of $\log(f_{60}/f_{100})$ in our sample (up to $10^{12.6} L_{\odot}$), though our colours are still warmer than those typical in less IR-luminous galaxies.

We compare the IR luminosity and the redshift distribution of ULIRGs with flux qualities of 1 (open circles in

Figure 10, 11, and 12) to those with flux qualities of 2 or 3 (filled circles). The mean IR luminosity for ULIRGs with flux qualities of 1 at 12 μm is not different from that for ULIRGs with flux qualities of 2 or 3 as seen in Figure 10. Similar results are found for ULIRGs at 25 μm and at 100 μm . The median redshift ($\bar{z}=0.230$) for ULIRGs with flux qualities of 1 at 12 μm is larger than that ($\bar{z}=0.163$) for ULIRGs with flux qualities of 2 or 3 at 12 μm . Similarly, the median redshifts for ULIRGs with flux qualities of 1 at 25 μm ($\bar{z}=0.236$) and at 100 μm ($\bar{z}=0.262$) are larger than those for ULIRGs with flux qualities of 2 or 3 at 25 μm ($\bar{z}=0.148$) and at 100 μm ($\bar{z}=0.196$).

4.3 Hyperluminous Infrared Galaxies

Of the 14 HLIRG candidates satisfying selection criteria of HLIRGs up to step (iii) in Section 2.2, all were excluded in further steps. However, we identified two HLIRGs, F01044–4050 and F09105+4108, in the course of NED Near Position Search for ULIRGs candidates at step (v) in Section 2.2. We list the 2 HLIRGs identified in this study in Table 5. Column (1) lists the *IRAS* object name in the FSC92. Columns (2) and (3) list the J2000.0 source position. Column (4), (5), (6) and (7) give the *IRAS* flux densities (and their errors) at 12 μm , 25 μm , 60 μm and 100 μm , respectively. The *IRAS* flux density quality at each band is given in Column (8). Column (9) lists the finally accepted redshift and Column (10) gives the IR luminosity calculated in this study. Log (LR) is given in the final Column. In Figure 13, we present 3' \times 3' grayscale images and contour plots extracted from the SuperCOSMOS scans of r_F survey plates (left panel), as well as those from the SDSS *gri* composite image and the SDSS *r*-band image (right panel) for the final sample of two HLIRGs. The identification procedure and properties of the HLIRGs are given in Appendix B of the electronic issue.

5 SUMMARY

We present a new sample of ULIRGs and HLIRGs found by cross-correlating the *IRAS* sources in FSC92 with the spectroscopic samples of galaxies in the SDSSDR4, 2dFGRSDRF and 6dFGSDR2. Our primary results are summarised below:

(i) We have identified 324 ULIRGs including 190 newly discovered ULIRGs in the regions of the sky covered by the SDSSDR4, 2dFGRSDRF and 6dFGSDR2. We increase the number of catalogued ULIRGs by about 30 per cent.

(ii) The reliability of the cross-correlation is estimated using the likelihood ratio method. We compute the likelihood ratio of each association for our sample of ULIRGs. The completeness of the final sample has been estimated using previously known ULIRGs in the redshift surveyed region. The incompleteness introduced by our identification procedure due to the cross-correlation using 3 σ error ellipse, and the selection using LR value and using the redshift quality parameter is estimated to be about 5 per cent.

(iii) The redshifts in our final sample run from $z=0.037$ to $z=0.517$ and the median value is $\bar{z}=0.223$, which is larger than that ($\bar{z}=0.184$) in previous ULIRG samples.

(iv) Two HLIRGs, F01044–4050 and F09105+4108, are found in the course of NED Near Position Search of ULIRGs candidates.

ACKNOWLEDGMENTS

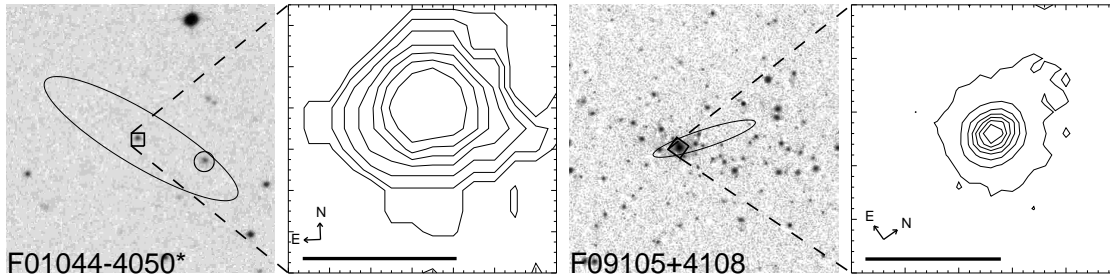
We would like to thank Dr. Woong-Seob Jeong and Jung-Hoon Kim for helpful discussions, and to anonymous referee for useful comments. H.S.H. and M.G.L. were supported in part by ABRL (R14-2002-058-01000-0) and the BK21 program of the Korean Government. K.H.L. acknowledges the support of the Royal Society RM/Korea/XF12003/16356. We would also like to thank all the people involved in creating the SDSS, 2dFGRS, 6dFGS, SuperCosmos surveys, and NED. Funding for the SDSS and SDSS-II has been provided by the Alfred P. Sloan Foundation, the Participating Institutions, the National Science Foundation, the U.S. Department of Energy, the National Aeronautics and Space Administration, the Japanese Monbukagakusho, the Max Planck Society, and the Higher Education Funding Council for England. The SDSS Web Site is <http://www.sdss.org/>. The SDSS is managed by the Astrophysical Research Consortium for the Participating Institutions. The Participating Institutions are the American Museum of Natural History, Astrophysical Institute Potsdam, University of Basel, University of Cambridge, Case Western Reserve University, University of Chicago, Drexel University, Fermilab, the Institute for Advanced Study, the Japan Participation Group, Johns Hopkins University, the Joint Institute for Nuclear Astrophysics, the Kavli Institute for Particle Astrophysics and Cosmology, the Korean Scientist Group, the Chinese Academy of Sciences (LAMOST), Los Alamos National Laboratory, the Max-Planck-Institute for Astronomy (MPIA), the Max-Planck-Institute for Astrophysics (MPA), New Mexico State University, Ohio State University, University of Pittsburgh, University of Portsmouth, Princeton University, the United States Naval Observatory, and the University of Washington. This research has made use of the NASA/IPAC Extragalactic Database (NED) which is operated by the Jet Propulsion Laboratory, California Institute of Technology, under contract with the National Aeronautics and Space Administration.

REFERENCES

- Arribas S., Colina L., 2002, *ApJ*, 573, 576
- Adelman-McCarthy J. K., et al., 2005, preprint (astro-ph/0507711)
- Allen D. A., Norris R. P., Meadows V. S., Roche P. F., 1991, 248, 528
- Borne K. D., Bushouse H., Lucas R. A., Colina L., 2000, *ApJ*, 529, 77
- Boyce P. J., et al., *ApJ*, 1996, 473, 760
- Bushouse H. A., et al., *ApJS*, 2002, 138, 1
- Canalizo G., Stockton A., 2001, *ApJ*, 555, 719
- Cao C., Wu H., Wang J. L., Hao C. N., Deng Z. G., Xia X. Y., Zou Z. L., 2006, *ChJAA*, 6, 197
- Clements D. L., Sutherland W. J., Saunders W., Efstathiou G. P., McMahon R. G., Maddox S., Lawrence A., Rowan-Robinson M., 1996a, *MNRAS*, 279, 459

Table 5. The Final Sample of HLIRGs

FSC NAME	RA (J2000)	Dec (J2000)	12 μ m (Jy)	25 μ m (Jy)	60 μ m (Jy)	100 μ m (Jy)	Flux Qual	final z	log L_{ir} (L_{\odot})	log(LR)
F01044-4050	01 06 44.9	-40 34 21	0.140(0.042)	0.155(0.039)	0.405(0.049)	0.655(0.203)	1231	0.584	13.19	0.648
F09105+4108	09 13 44.0	40 56 34	0.129(0.031)	0.333(0.033)	0.525(0.042)	0.437(0.109)	2331	0.442	12.97	0.191


Figure 13. Similar to the Figure 1, except for two HLIRGs, F01044-4050 (left two panels) and F09105+4108 (right two panels), identified in this study. The small circle in the first panel indicate the position of 6dF J0106412-403437.

- Clements D. L., Sutherland W. J., McMahon R. G., Saunders W., 1996b, MNRAS, 279, 477
 Clements D. L., Saunders W. J., McMahon R. G., 1999, MNRAS, 302, 391
 Clowes R. G., Campusano L. E., Leggett S. K., Savage A., 1995, MNRAS, 275, 819
 Cohen M., Schwartz D. E., Chokshi A., Walker R. G., 1987, AJ, 93, 1199
 Colless M. et al., 2001, MNRAS, 328, 1039
 Cui J., Xia X.-Y., Deng Z.-G., Mao S., Zou Z.-L., 2001, AJ, 122, 63
 Darling J., Giovanelli R., 2001, AJ, 121, 1278
 Darling J., Giovanelli R., 2002, AJ, 124, 100
 Duc P.-A., Mirabel I. F., Maza J., 1997, A&AS, 124, 533
 Farrah D., et al., 2001, MNRAS, 326, 1333
 Farrah D., Afonso J., Efstathiou A., Rowan-Robinson M., Fox M., Clements D., 2003, MNRAS, 343, 585
 Farrah D., Surace, J. A., Veilleux S., Sanders D. B., Vacca W. D., 2005, ApJ, 626, 70
 Fisher K. B., Huchra J. P., Strauss M. A., Davis M., Yahil A., Schlegel D., 1995, ApJS, 100, 69
 Franceschini A., et al., 2003, MNRAS, 343, 1181
 Genzel R. et al., 1998, ApJ, 498, 579
 Genzel R., Cesarsky C. J., 2000, ARA&A, 38, 761
 Genzel R., Tacconi L. J., Rigopoulou D., Lutz D., Tecza M., 2001, ApJ, 563, 527
 Goto T., 2005, MNRAS, 360, 322
 Houck, J. R. et al., 2005, ApJ, 622, L105
 Hutchings J. B., Neff S. G., 1988, AJ, 96, 1575
 IRAS Point Source Catalogue, Version 2, 1988, Washington: GPO (PSC)
 Jones D. H. et al., 2004, MNRAS, 355, 747
 Jones D. H., Saunders W., Read M., Colless M., 2005, PASA, 22, 277
 Kessler, M. F. et al., 1996, A&A, 315, L27
 Kewley L. J., Heisler C. A., Dopita M. A., Lumsden S., 2001, ApJS, 132, 37
 Kim D.-C., Sanders D. B., 1998, ApJS, 119, 41
 Kim D.-C., Veilleux S., Sanders D. B., 2002, ApJS, 143, 277
 Kleinmann S. G., Hamilton D., Keel W. C., Wynn-Williams C. G., Eales S. A., Becklin E. E., Kuntz K. D., 1988, ApJ, 328, 161
 Kormendy J., Sanders D. B., 1992, ApJ, 390, 53
 Lawrence A., Rowan-Robinson M., Leech K., Jones D. H. P., Wall J. V., 1989, MNRAS, 240, 329
 Lawrence A., et al., 1999, MNRAS, 308, 897
 Leech K. J., Rowan-Robinson M., Lawrence A., Hughes J. D., 1994, MNRAS, 267, 253
 Lonsdale C. J. et al., 1998, in McLean B. J., Golombek D. A., Hayes J. J. E., Payne H. E., eds, Proc. IAU Symp. 179, New Horizons from Multi-Wavelength Sky Surveys. Kluwer, Dordrecht, p. 450
 Lonsdale C. J., Farrah D., Smith H. E., 2006, preprint (astro-ph/0603031)
 Lutz, D., Spoon, H. W. W., Rigopoulou, D., Moorwood, A. F. M., Genzel, R., 1998, ApJ, 505, L103
 Lutz D., Veilleux S., Genzel R., 1999, ApJ, 517, L13
 Lutz D., Valiante E., Sturm E., Genzel R., Tacconi L. J., Lehnert M. D., Sternberg A., Baker A. J., 2005, ApJ, 625, L83
 Masci F. J. et al., 2001, PASP, 113, 10
 Mihos J. C., Bothun G. D., 1998, ApJ, 500, 619
 Moshir M. et al., 1992, Explanatory Supplement to the IRAS Faint Source Survey, Version 2, JPL D-10015 8/92 (Pasadena: JPL) (FSC92)
 Murphy T. W., Jr., Armus L., Matthews K., Soifer B. T., Mazzarella J. M., Shupe D. L., Strauss M. A., Neugebauer G., 1996, AJ, 111, 1025
 Neff S. G., Hutchings J. B., 1992, AJ, 103, 1746
 Neugebauer G. et al., 1984, ApJ, 278, L1
 Norberg P. et al., 2002, MNRAS, 336, 907
 Pasquali A., Kauffmann G., Heckman T. M., 2005, MNRAS, 361, 1121
 Ptak A., Heckman T., Levenson N. A., Weaver K., Strickland D., 2003, ApJ, 592, 782
 Rigopoulou D., Spoon H. W. W., Genzel R., Lutz D., Moorwood A. F. M., Tran Q. D., 1999, AJ, 118, 2625

- Rowan-Robinson M., 2000, MNRAS, 316, 885
- Sanders D. B., Mirabel I.F., 1996, ARA&A, 34, 749
- Sanders D. B., Soifer B. T., Elias J. H., Madore B. F., Matthews K., Neugebauer G., Scoville N. Z., 1988a, ApJ, 325, 74
- Sanders D. B., Soifer B. T., Elias J. H., Neugebauer G., Matthews K., 1988b, ApJ, 328, 35
- Sanders, D. B., Egami, E., Lipari, S., Mirabel, I. F., Soifer, B. T., 1995, AJ, 110, 1993
- Sanders D. B., Mazzarella J. M., Kim D.-C., Surace J. A., 2003, AJ, 126, 1607
- Saunders W. et al., 2000, MNRAS, 317, 55
- Soifer B. T., Sanders D. B., Neugebauer G., Danielson G. E., Lonsdale C. J., Madore B. F., Persson S. E., 1986, ApJ, 303, L41
- Soifer B. T., Sanders D. B., Madore B. F., Neugebauer G., Danielson G. E., Elias J. H., Lonsdale C. J., Rice W. L., 1987, ApJ, 320, 238
- Soifer B. T., Boehmer L., Neugebauer G., Sanders D. B., 1989, AJ, 98, 766
- Soifer B. T., & Neugebauer G., 1991, AJ, 101, 354
- Stanford S. A., Stern D., van Breugel W., De Breuck C., 2000, ApJS, 131, 185
- Strauss M. A., Davis M., Yahil A., Huchra J. P., 1990, ApJ, 361, 49
- Strauss M. A., Huchra J. P., Davis M., Yahil A., Fisher K. B., Tonry J., 1992, ApJS, 83, 29
- Surace J. A., 1998, PhD thesis, Univ. Hawaii
- Surace J. A., Sanders D. B., Vacca W. D., Veilleux S., Mazzarella J. M., 1998, ApJ, 492, 116
- Surace J. A., Sanders D. B., Evans A. S., 2000, ApJ, 529, 170
- Sutherland W., Saunders W., 1992, MNRAS, 259, 413
- M., 1998, ApJ, 492, 116
- Tran, Q. D. et al., 2001, ApJ, 552, 527
- Tacconi L. J., Genzel R., Lutz D., Rigopoulou D., Baker A. J., Iserlohe C., Tecza M., 2002, ApJ, 580, 73
- Veilleux S., Kim D.-C., Sanders D. B., Mazzarella J. M., Soifer B. T., 1995, ApJS, 98, 171
- Veilleux S., Kim D.-C., Sanders D. B., 1999, ApJ, 522, 113
- Veilleux S., Kim D.-C., Sanders D. B., 2002, ApJS, 143, 315
- Verma A., Charmandaris V., Klaas U., Lutz D., Haas, M., 2005, Space Sci. Rev., 119, 355
- White G. L., Jauncey D. L., Savage A., Wright A. E., Batty M. J., Peterson B. A., Gulkis S., 1988, ApJ, 327, 561
- Werner M. W. et al., 2004, ApJS, 154, 1
- Yan L., Chary R., Armus L., Teplitz H., Helou G., Frayer D., Fadda D., Surace J., Choi P., 2005, ApJ, 628, 604
- York D. G. et al., 2000, AJ, 120, 1579
- Zheng Z., Wu H., Mao S., Xia X.-Y., Deng Z.-G., Zou Z.-L., 1999, A&A, 349, 735
- Zhenlong Z., Xiaoyang X., Zupan D., Hongjun S., 1991, MNRAS, 252, 593